Microgravity Science and Technology (2022) 34: 38
https://doi.org/10.1007/s12217-022-09957-0

ORIGINAL ARTICLE

Design and Validation of Closed Two-phase Thermosyphon Loop in Lunar Gravity Environment during China Lunar Project CE-4

Yuandong Guo[1] · Lu Wang[2] · Jianyin Miao[2] · He Zhang[2] · Youwei Zhang[2] · Hongxing Zhang[2] · Jianxin Chen[2] · Yawei Xu[2] · Yalong Wang[2] · Jianfu Zhao[3,4]

Received: 21 March 2022 / Accepted: 5 May 2022 / Published online: 31 May 2022

Abstract

The structural design, heat transfer capability analysis, ground equivalent validation, and on-orbit flight of the two-phase fluid loop based on flat-plate evaporation module of the Chang'e-4 detector are introduced. Within the temperature range of -30 ℃ ~ -10 ℃, the designed two-phase fluid loop has a heat transfer capacity of greater than 200 W. An equivalent test prototype is designed and manufactured to examine the heat transfer performance of the two-phase fluid loop under the ground condition of 1 *g*. The driving force of the equivalent test prototype is less than that of the flight prototype, while the flow resistance is equivalent to that of the flight prototype. The test heat transfer capacity is smaller than that of the flight prototype on the lunar surface. According to the equivalent test prototype, the heat transfer capacity is no less than 130 W, which meets the requirements of Chang'e-4. During the 14-moon day-night cycle, the temperature of the two-phase fluid loop gradually decreased to an equilibrium value of -10 °C. During the wake-up process of the detector in moon day, the control valve was closed, and the temperature of the flat-plate evaporation module rose rapidly, indicating that the function of blocking heat transfer is normal.

Keywords Gravity driven · Thermosyphon · Validation · Experiment · Operating characteristics

Abbreviations

ΔP_{driven}	Maximum capillary pressurePa
ΔP_{eva}	Pressure drop in evaporatorPa
ΔP_{vl}	Pressure drop in vapor linePa
ΔP_{con}	Pressure drop in condenser pipelinePa
ΔP_{ll}	Pressure drop in liquid linePa
ΔP_{local}	Local pressure lossPa
ρ	Densitykg/m^3
α	Gravitational accelerationkg/m^{2}s
Δh	Height differencem
f	Fraction factor
L	Lengthm
D	Diameterm
u	Flow velocitym/s
Re	Reynolds number
$\frac{dP}{dz}$	Pressure drop per meterPa/m
$\frac{UA}{L}$	Equivalent heat transfer coefficient W/m^2 • K
Nu	Nusselt number
λ_f	Thermal conductivity W/m • K
h	Convective heat transfer coefficient W/m^2 • K
A	External surface area m^2
T	Temperature °C
m	Masskg
c_p	Thermal capacity J/kg • K
ε	Surface emissivity
σ	Stefan Boltzmann constant $5.67 \times 10^8 W/m^2K^4$
Q	Heat loadW
μ	ViscosityPa • s
Pr	Prandtl number

Subscripts

l	Liquid
v	Vapor

✉ Lu Wang
wanglulkdd@163.com

[1] Laboratory of Fundamental Science On Ergonomics and Environmental Control, School of Aeronautic Science and Engineering, Beihang University, Beijing 100191, China

[2] Beijing Key Laboratory of Space Thermal Control Technology, Beijing Institute of Spacecraft System Engineering, China Academy of Space Technology, Beijing 100094, China

[3] CAS Key Laboratory of Microgravity (National Microgravity Laboratory), Institute of Mechanics, Chinese Academy of Sciences, Beijing 100190, China

[4] School of Engineering Science, University of Chinese Academy of Sciences, Beijing 100049, China

sp	Single-phase
tp	Two-phase
o	Outer
i	Inner
a	Ambient
sat	Active zone
sink	Cold gas reservoir
f	Fluid
s	Solid

Nomenclatures

CAST	China Academy of Space Technology
CTPTL	Closed two-phase thermosyphon loop
CE-4	Chang'e-4
CE-3	Chang'e-3
RHU	Radioisotope Heat Unit
RTG	Radioisotope Thermoelectric Generator
Eva	Evaporator
VL	Vapor line
Con	Condenser
CC	Compensation chamber
CV	Control valve
LL	Liquid line
OD/ID	Outer/inner diameter

Introduction

Since 1950s, mankind has never stopped exploring the moon and other extraterrestrial objects. All countries are conducting lunar exploration research with the hope of building a survivable lunar station (Reitz et al. 2021; Fateri et al. 2019). However, many technological challenges such as the survival ability of the equipment arise during the planning for a robotic or manned lunar mission fully operational during the lunar night (Benaroya 2017; Fraser 2012; Palos et al. 2020). In past attempts at lunar exploration, many technologies have been used in thermal control systems, such as multiple insulation layers (Kim 2020; Plachta et al. 2012), single-phase, two-phase (Simonsen et al. 1992), and heat pumps (Sridhar and Gottmann 1996). Stephan (2009) conducted a very brief overview of the Altair vehicle and mission architecture, which is the next generation moon lander. And the two-phase fluidic loop is chosen for the thermal control system.

The thermosyphon loop is a widely used two-phase heat transfer device that utilizes evaporation and condensation of working fluid for heat transfer. Specifically, it utilizes gravity, or to be more exact, buoyancy rather than a pump or capillary action to drive the circulation of working fluid. It has been adopted for the thermal control system of terrestrial applications, such as electronic cooling, telecommunication devices, energy storage systems, thermoelectric power generators, and various heating or cooling applications (Li et al. 2014; Samba et al. 2013; Sarno et al. 2013).

Samba et al. (2013) tested a pentane thermosyphon loop for cooling a telecommunication cabinet to substitute forced convection, finding that the optimal fill ratio is about 9.2% with thermal resistance at minimum operating temperature. Tong et al. (2017) experimentally studied an R744-based thermosyphon loop with two parallel evaporators, and focused on the different heat powers onto evaporators with varying thermal performance. In order to reduce the flow instability in loop thermosyphon, Khodabandeh and Furberg (2010a, b) designed a nano-porous structure evaporator with R134a as refrigerant because it can obtain a higher heat flux compared with smooth surface evaporators. He et al. (2013, 2014) investigated the effects of non-condensable gas on a thermosyphon loop with ammonia as working fluid, as well as the startup and steady-state operations. Zhang et al. (2018) tried to develop a performance evaluation method for the two-phase thermosyphon loop and noted that the thermosyphon would malfunction due to small height difference and small driving force. Sukchana and Pratinthong (2017) investigated the thermal performance of an R134a thermosyphon loop with the adiabatic section of flexible hose, and the worsening result at a tilt angle meant the bad influence of small height difference. Zhang et al. (2020) investigated a closed-loop two-phase thermosyphon to improve the heat transfer in the latent heat storage devices, and pointed out that the filling ratios would play an important role in the thermal performance.

However, the lunar gravity is about 1/6 *g*, meaning the design method, working performance, and ground validation would be different from their counterparts on the earth. The working limits would decrease, and the thermal resistance would rise, due to the heat transfer mechanism on the moon (Hu et al. 2009; Zhao et al. 2001). Therefore, many attempts have been made to tilt the system by flying on a low-gravity aircraft (Jaworske et al. 2011). But the experiment duration is usually very short, which makes it impossible to reach a stable operating state. Thus, the ground validation prototype should be designed and tested to ensure normal operation on the moon.

To the best of our knowledge, few studies are concerned about the loop thermosyphons driven by reduced gravity, and almost no literatures address the ground validation. In the second phase of China's lunar exploration project, a 1/6 *g* gravity-driven thermosyphon loop was invented in China Academy of Space Technology (CAST) around the world (Zhang et al. 2014; Zhao et al. 2015). The development and application of the closed two-phase thermosyphon loop (CTPTL) provide a brand and new thermal control design idea for spacecraft detectors. It can solve the thermal control problems during dormant time that are commonly encountered in deep space exploration. More attempt should

be conducted to obtain more operating details and general principle of the system. Thus, a new CTPTL is designed and adopted for the lunar detector based on the previous work. The design procedure and experimental validation on ground and lunar surface are covered in this paper. Some special operating characteristics of the CTPTL are presented and analyzed.

Challenge and Structure Design

Functional and Performance Requirements

Chang'e-4 (CE-4) detector has achieved the first soft landing on the back of the moon and patrol survey. CE-4 fully inherits the design methodology of thermal control for Chang'e-3 (CE-3) moon-night survival and uses the CTPTL system to keep the lunar probe at appropriate temperature. CE-3 completed the engineering mission, but was limited by resources to obtain sufficient lunar surface measurement and data. While CE-3 utilizes the Radioisotope Heat Unit (RHU) for heating during the moon night, CE-4 detector uses the Radioisotope Thermoelectric Generator (RTG), taking into account the power generation and heating requirements of the moon night. Different from RHU, RTG achieves the heat transfer process by means of a temperature differential power generator. The difference between heat sources of CE-3 and CE-4 is shown in Fig. 1, where the shape determines the structure of the evaporators. Due to the shape of RHU, the evaporator of thermosyphon loop is designed as a cage structure for heat collection as shown in Fig. 1. However, the heating mechanical interface of RTG is a large plane, indicating a flat structure of the evaporator. The test results show that the thermal resistance of CE-4 CTPTL is reduced by almost 50% compared to CE-3.

The functional requirements of the CE-4 detector for the CTPTL system are as follows. During the moon day, the CTPTL is in the dormant state, where the heat of the RTG is thermally isolated from the detector through closing the control valves. The RTG and evaporator could rebalance at a relatively higher but safe temperature. During the moon night, the CTPTL is in the operating state, where the heat of the RTG is transferred to the inside of the detector. The requirements for heat transfer capacity and temperature difference of the thermosyphon loop are shown in Table 1.

Table 1 Requirements for the CTPTL system

Working temperature /℃	Heat transfer capacity /W	Temperature difference /℃
-30	≥55	≤20
-20	≥70	≤15
-10	≥90	≤12

General Layout and Design of Components

According to the structural layout and heat transfer capacity requirements of the CE-4 detector, the overall structure of the CTPTL is shown in Fig. 2. It consists of a flat-plate evaporator (Eva), a vapor line (VL), a condenser (Con), a compensation chamber (CC), two control valves (CVs), and a liquid line (LL). The working medium is ammonia. In the lunar gravity direction, the compensation chamber is higher than the flat-plate evaporator, forming a driving force for the operation of the fluid loop. The flat-plate evaporator and RTG are coupled to absorb heat. The condenser is embedded in the structural board on the detector, and the absorbed heat is supplied to the detector through the thermal radiation of the structural board. During the moon day, the control valves are closed, blocking the compensation chamber from supplying the liquid working medium into the flat-plate evaporator, and the two-phase fluid loop is adiabatic. During the moon night, the control valves are turned on, and the liquid working medium flows into the flat-plate evaporator and absorbs heat from RTG. Then it turns into vapor and flows into the condenser pipeline along the vapor line. The vapor condenses into liquid and releases heat to the structural plate. Eventually it returns to the reservoir to form a cycle.

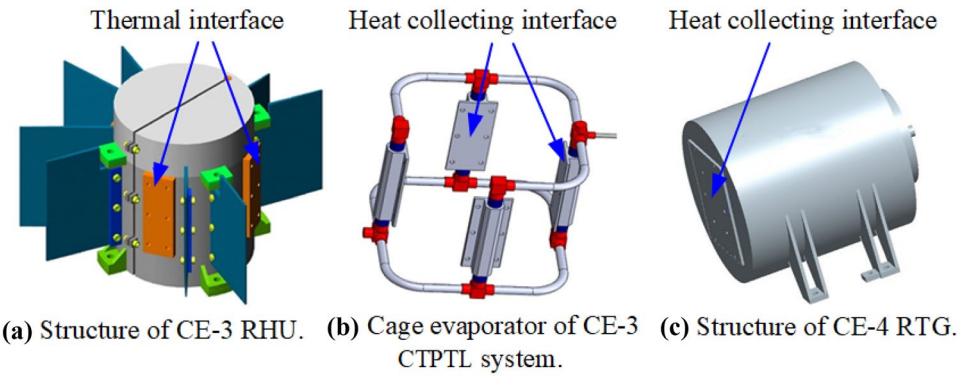

Fig. 1 The comparison between the thermal units of CE-3 and CE-4

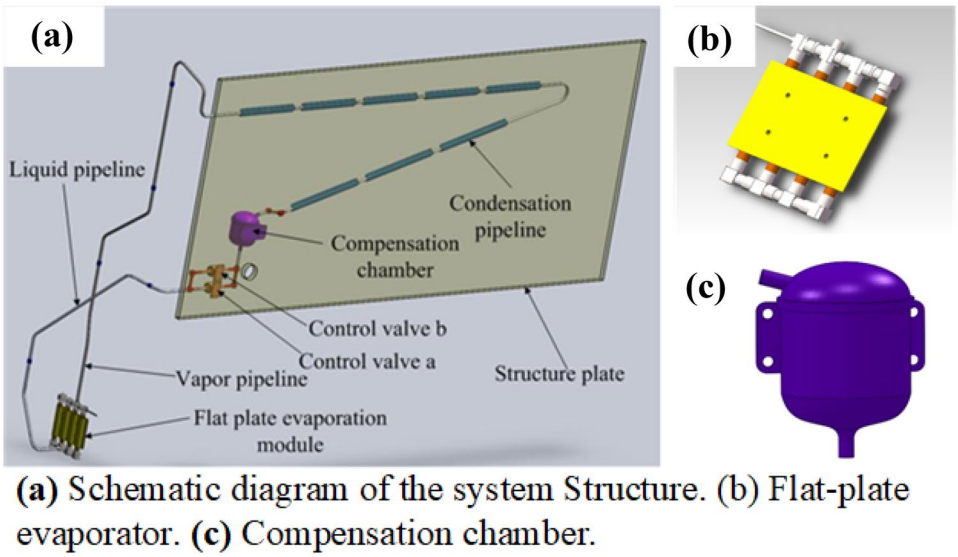

Fig. 2 Structure of 1/6 *g* closed two-phase thermosyphon loop

(a) Schematic diagram of the system Structure. (b) Flat-plate evaporator. **(c)** Compensation chamber.

The flat-plate evaporator consists of four evaporators filled with mesh, aluminum saddles, and joints, as shown in Fig. 2(b). The four evaporators are coupled to the aluminum saddles by braze welding. The working medium in the mesh evaporators absorbs heat power and remove the thermal load from the RTG by phase change. The mesh is made of stainless steel, which can be welded onto the inner surface of the evaporator. The evaporators are also made of stainless steel, with the detailed diameter shown in Table 2. The material of the saddle is aluminum, whereas the material of the vapor line and liquid line is stainless steel.

The condenser is composed of a condenser pipeline and condensation fins, which are coupled by thermos isostatic means, as shown in Fig. 2a. The material of the condenser pipeline is stainless steel, whereas the material of the condensation fins is aluminum.

According to the operating principle and large engineering experience, the volume of the compensation chamber and the mass of ammonia should be matched and designed to meet the following constraints:

Table 2 Basic parameters of the thermosyphon loop

Components	Flight product parameters	Ground product parameters
OD/ID × Length of evaporator/mm	10/7 × 90	
Length × Width of wick/mm	120/80	
OD/ID × Length of vapor line/mm	6/4.4 × 1260	
OD/ID × Length of condenser/mm	6/4.4 × 2200	
OD/ID × Length of liquid line/mm	6/4.4 × 1320	
Volume of CC/mL	200	600
Charging mass/g	106	600

1. Given that the flat-plate Eva, VL, LL, two CVs and Con are filled with liquid at low operating temperature of -50℃, the proportion of the liquid working medium in the CC should be no less than 10%;
2. Given that the Eva, VL, LL, two CVs and Con are filled with vapor at high operating temperature of 70 °C, the proportion of the liquid working fluid in the CC should not exceed 100%;
3. Under the storage condition of high temperature 90 °C, the liquid working fluid occupies no more than 90% of the total volume of the fluid loop. It can secure the system at high temperature.

Due to the difference between the gravity conditions of 1 *g* on the earth and 1/6 *g* on the moon, it is impossible to test the heat transfer capacity of the two-phase fluid loop directly on the earth, unless the test is conducted on a parabolic flight for a short time (Pletser 2019). Therefore, an equivalent test prototype for the heat transfer performance is shown in Fig. 3. The ground validation test should follow two principles as follows:

(a) Under all working conditions, the actual driving force on the earth should be lower than on the lunar surface to ensure the validity of the ground experiment;
(b) Considering the flow resistance increase on the lunar surface, the ground driving force should not be too conservative in order to ensure the success in the ground experiment.

Therefore, the ground simulation experiment method of driving force is detailed as follows:

(i) In order to simulate the experimental situation for CTPTL system, the height difference between the

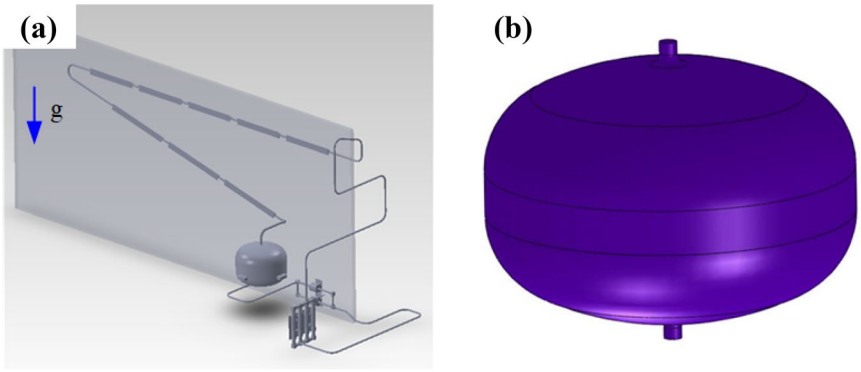

Fig. 3 The structure of the equivalent test prototype and compensation chamber

(a) Schematic diagram of the 1*g* equivalent system structure. **(b)** Compensation chamber.

liquid surface in the compensation chamber and the bottom of the flat-plate evaporator is reduced to 1/6 of moon height contrast. The structure of the flat-plate evaporator, condenser, transport lines, and control valves are exactly the same as that of the flight product.

(ii) In order to reduce the drastic change of the pressure head with the change of liquid level in the reservoir, the cross-sectional area of the reservoir is increased by 6 times in the ground simulation experiment. This can also avoid the failure and invalidity of the experiment due to over-verification and under-verification. Furthermore, under different working conditions, the height difference between the reservoir and the evaporator will vary with operating temperature. Increasing the cross-sectional area of the reservoir can keep the flight height difference 6 times of the ground equivalent working condition. Figure 4 shows the comparison between the two prototypes about driving heights.

According to the above design constraints, the final volume of the CC is designed as 200 mL and the working medium mass as 106 g. The detailed parameters are listed in the following table.

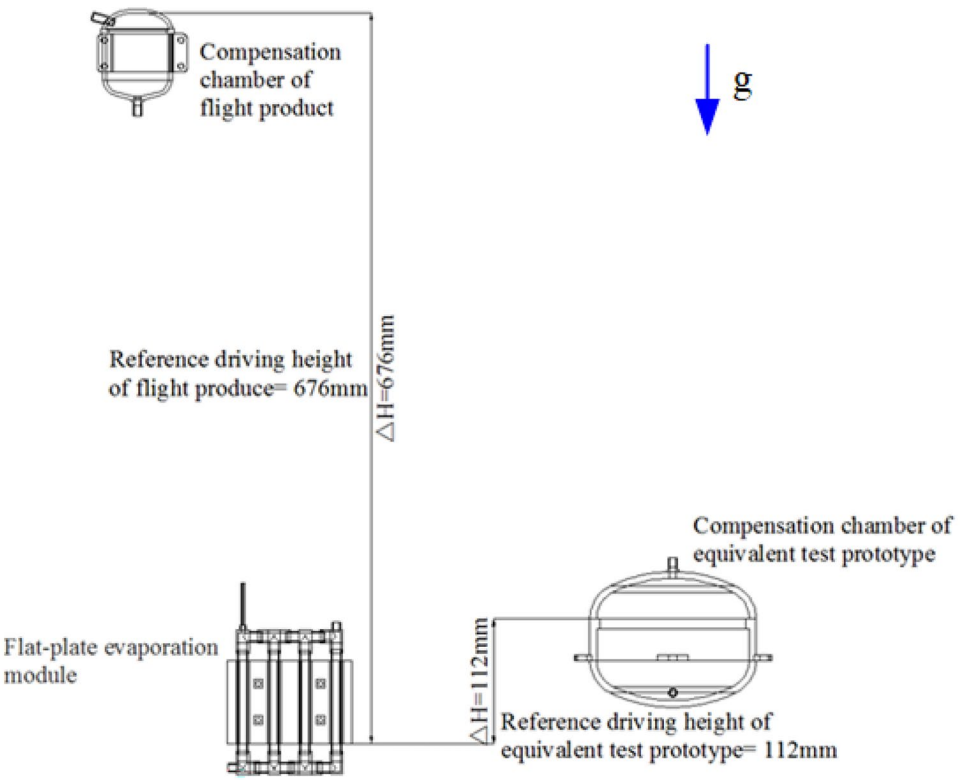

Fig. 4 Reference driving heights of the flight product and the equivalent test prototype

Thermal Modeling and Prediction

Assumption

A simulation model built for the thermosyphon loop can be used to predict the thermal performance of ground and flight products. The main purpose is to analyze the steady-state operating characteristics, that is, the relations between system temperature, heat load, and ambient temperature. In the steady-state model, the ambient temperature is constant for condenser heat transport. The specific assumptions are made as follows:

(a) The one-dimensional model is built due to the extremely small diameter-to-length ratio.
(b) The influence of the pressure drop along the way on the physical property parameters is ignored.
(c) The vapor line, liquid line, and compensation chamber are covered with insulation materials with a small heat leakage from the ambient.
(d) The flow resistance of the four parallel evaporators is consistent with the heat transfer characteristics, and the heat load on the wall of the evaporation tube is evenly distributed along the way, ignoring the oscillation effect between the evaporators.

Steady-state Model of the CTPTL

The heat transfer capacity of a two-phase fluid loop depends on the match between driving force and flow resistance. The driving force stems from the pressure generated by the lunar gravity and height difference between the compensation chamber and the flat-plate evaporator; the flow resistance stems from the pressure drop due to the working fluid flowing in the pipeline, including the pressure drop along all the components and the local pressure drop. The formula is given as follows:

$$\Delta P_{driven} = \Delta P_{eva} + \Delta P_{vl} + \Delta P_{con} + \Delta P_{ll} + \Delta P_{local} \tag{1}$$

The driven pressure can be calculated from Eq. (2) while the operating temperature is settled down.

$$\Delta P_{driven} = \left(\rho_l - \rho_v\right)\alpha\Delta h \tag{2}$$

where ΔP_{driven} represents the maximum capillary pressure, and ΔP_{eva}, ΔP_{vl}, ΔP_{con}, ΔP_{ll}, and ΔP_{local} represent the pressure drops in the evaporator, vapor line, condenser pipeline, liquid line, and local pressure loss, respectively. ρ_l and ρ_v represent the density of liquid and of vapor, respectively. α is the gravitational acceleration on the Earth and Moon, being 9.8 kg/m^{2}s and 1.63 kg/m^{2}s, respectively. Δh is the height difference across vapor–liquid interface of the compensation chamber and evaporator.

Table 3 Heat transfer and pressure drop correlations

	Formulae
Friction pressure drop (single-phase)	$\Delta P_{sp} = f\left(\frac{L}{D}\right)\frac{\rho u^2}{2}$
	$f = \begin{cases} 64Re^{-1} & Re < 2300 \\ 0.00063Re^{0.5} & 2300 < Re < 4000 \\ 0.316Re^{-0.25} & Re > 4000 \end{cases}$
Friction pressure drop (two-phase)	$\left(\frac{dP}{dz}\right)_{tp} = \Phi_l^2\left(\frac{dP}{dz}\right)_l$
	$\Phi_l^2 = 1 + \frac{C}{X} + \frac{1}{X^2}$
	$X^2 = \left(\frac{dP}{dz}\right)_l / \left(\frac{dP}{dz}\right)_v$
Heat transfer coefficient (single-phase)	$(\frac{UA}{L})_{f-a} = \left\{\frac{1}{Nu\bullet\lambda_f\pi} + \frac{1}{2\lambda_s\pi}\ln(\frac{D_o}{D_i}) + \frac{1}{(h_oA_o/L)_a}\right\}^{-1}$
	$T_{f-o} = T_a + (T_{f-i} - T_a)\bullet\exp\left[-\frac{(UA/L)_{f-a}}{mc_p}L\right]$
	$Nu = \begin{cases} 3.66 & laminar, constant\ wall\ temperature \\ 4.36 & aminar, constant\ heat\ flux \\ 0.023Re^{0.8}Pr^n & fully\ developed\ turbulence \end{cases}$
	Boundary condition:$k_s\frac{\partial T}{\partial z} = \varepsilon\sigma\left(T^4 - T_a^4\right)$
Heat transfer coefficient (two-phase)	$(\frac{UA}{L})_{f-s} = \left\{\frac{1}{h_{2\phi}\pi D_i} + \frac{1}{2\lambda_s\pi}\ln(\frac{D_o}{D_i}) + \frac{1}{(h_oA_o/L)_s}\right\}^{-1}$
	$L_{2\phi} = \frac{Q}{T_{sat}-T_{sink}}\int_{x_i}^{x_o}(\frac{UA}{L})_{f-s}dx$
	$h_{2\phi} = h_{lo}\left[1 + 1.28x^{0.817}\left(\frac{\rho_l}{\rho_v}\right)^{0.3685}\left(\frac{\mu_l}{\mu_v}\right)^{0.2363}\left(1 - \frac{\mu_l}{\mu_v}\right)^{2.144}Pr_l^{-0.1}\right]$

The formulae for pressure drop and heat transfer in each component are listed in * MERGEFORMAT Table 3.

The single-phase pressure drop in the pipe is calculated by Darcy-Weisbach formula, the two-phase flow friction loss by Lockheed-Martinelli formula (Lockhart 1949). The flow pressure drop in single phase could be calculated according to the flow state such as laminar and turbulent flows. The calculation of two-phase flow adopts separating flow model. The heat transfer in each component can be divided into single-phase and two-phase conditions similarly. The thermal operating parameters can be solved with total equivalent heat transfer coefficient $\frac{UA}{L}$ and the thermodynamic properties. Thus, the outlet temperature could be calculated by energy conversion considering the boundary conditions. And the condensation heat transfer coefficient in the tube can be calculated by Dittus-Boelter (1985) and Shah (2016) formulae. Therefore, the heat exchange in vapor line, liquid line, and single-phase zone of condenser can be obtained, and the two-phase distance and condenser outlet vapor quality can be calculated. The outlet state of condenser should be saturated or subcooled liquid to guarantee stable operation.

The flowchart of the steady-state simulation is shown in Fig. 5. In the simulation, the component parameters and boundary conditions are input and some operating values of the thermosyphon loop are supposed firstly. Then the relevant thermophysical properties can be obtained from NIST Refprop (Lemmon et al. 2018). The heat transfer and pressure drop are calculated for each element. Finally, the heat transfer capacity and saturation temperature can be determined through cyclic verification of the key parameters.

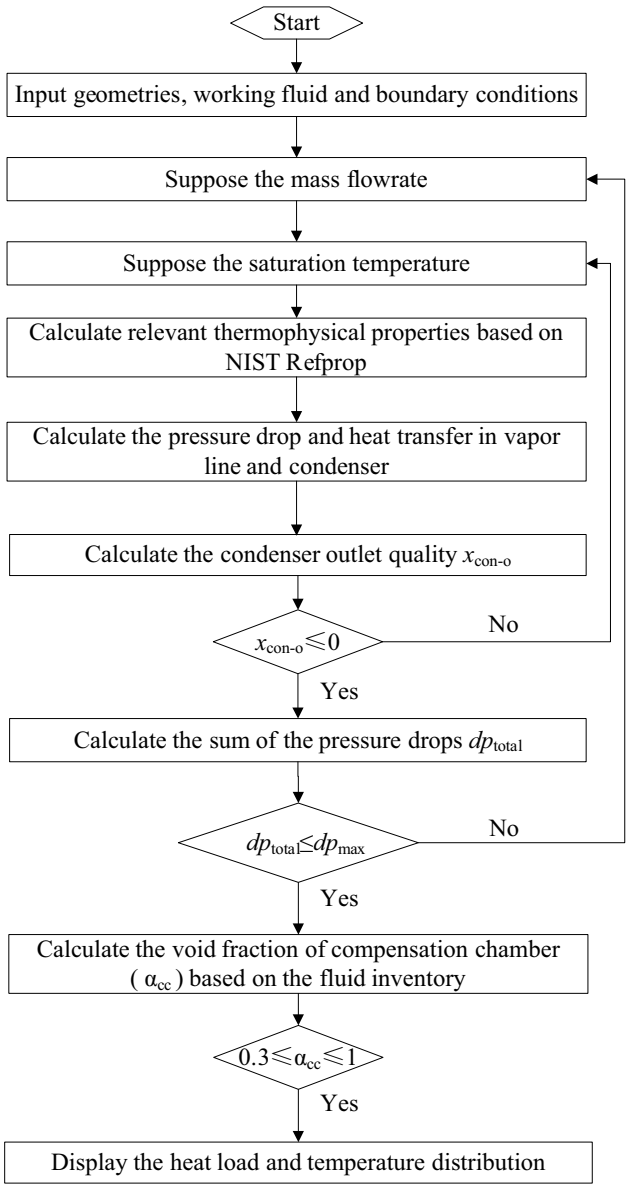

Fig. 5 Flowchart of steady-state simulation

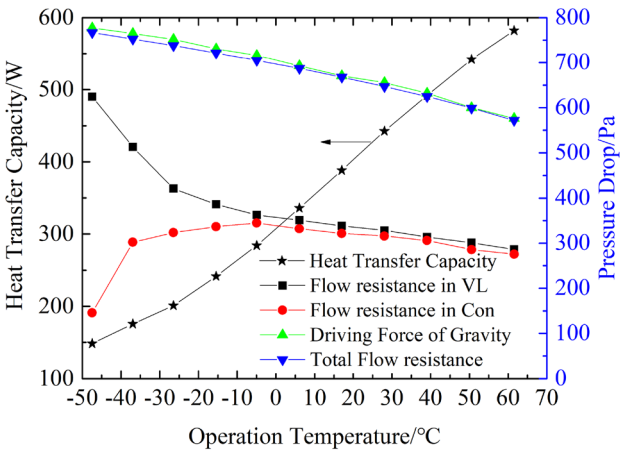

Fig. 6 Curve of heat transfer capacity of CTPTL at different temperatures

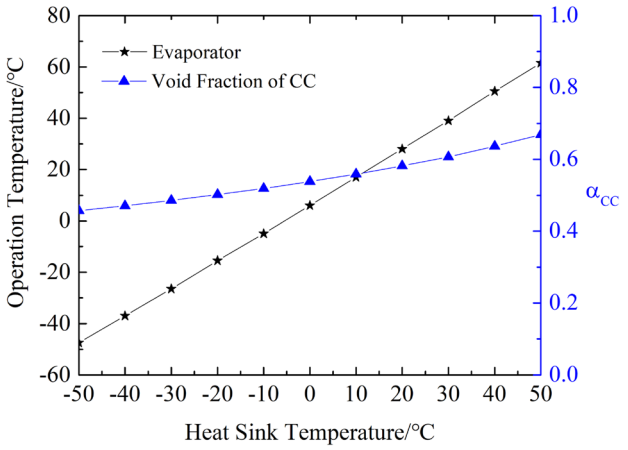

Fig. 7 Operating temperature and void fraction of CC under different heat sink temperature

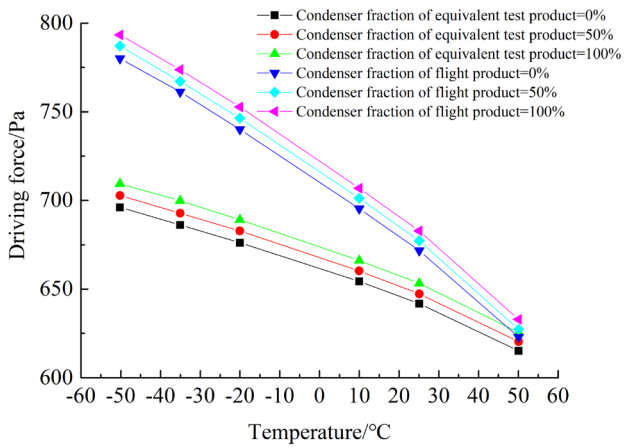

Fig. 8 Theoretical driving forces of flight product and equivalent test prototype

Zhao (2010) noted that under the small diameter and small flowrate condition, the friction loss in two-phase flow is independent of gravity. Thus, the model is used to calculate the thermal performance of the moon flight product, the Lockheed-Martinelli formula is still adopted for calculation. And the heat transfer coefficient in reduced-gravity condition can be calculated by correlations.

Theoretical Analysis and Discussion

Heat Transfer Capacity

In the temperature range of -50℃ ~ 50℃, the curve of the heat transfer capacity of the two-phase fluid loop with temperature is shown in Fig. 6. The heat transfer capacity is reached when the driving force of gravity no longer supports the total flow resistance in each component. It can be seen that the heat transfer capacity of the thermosyphon loop increases monotonically with the increase of operating temperature. In the temperature range of -30° C ~ 10 °C, the heat transfer capacity may exceed 200 W, which meets the heat transfer capacity requirements of CE-4 for the two-phase fluid loop. Figure 6 also shows the variation of driving force of gravity at different operating temperatures. The driving force decreases as the operating temperature increases due to the dropping gas–liquid density difference. The vapor density increases while the liquid density decreases as the saturation temperature rises, leading to the variations of flow resistance of VL and Con as shown in Fig. 6. When the inner diameter of evaporator is relatively large of 7 mm resulting a small pressure drop, and the sum of the flow resistance in the VL and Con accounts for more than 97% of the total flow resistance.

Fig. 9 Locations of the temperature measurement points of the equivalent test prototype

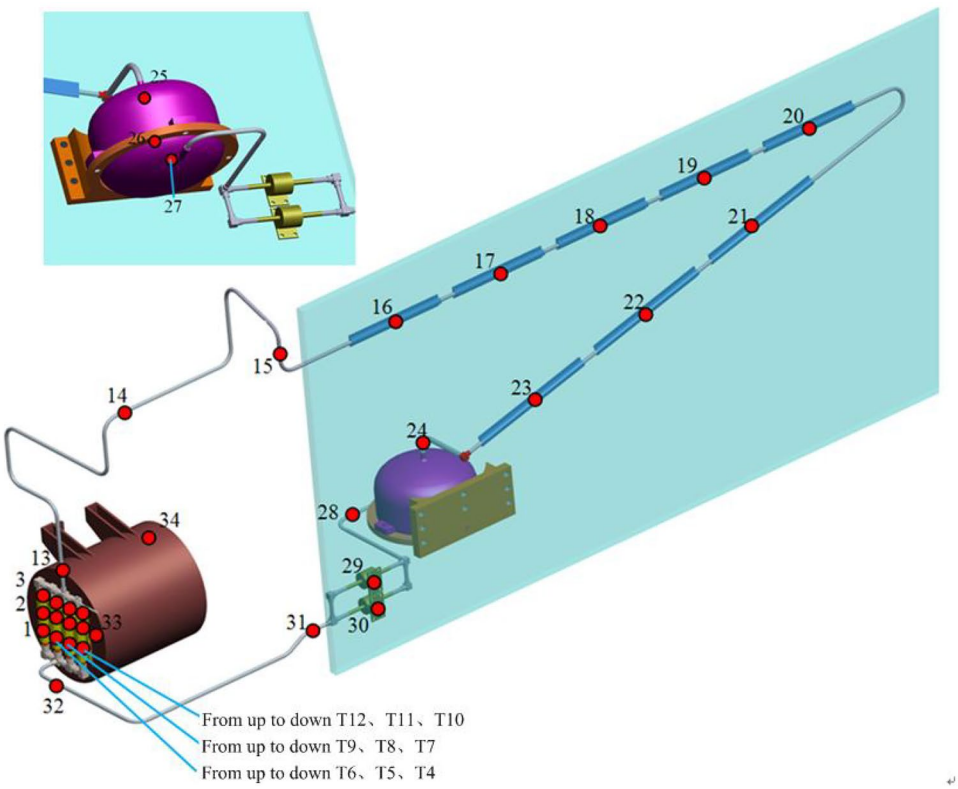

Figure 7 shows the variations of operating temperature and void fraction of compensation chamber at different heat sink temperatures. The steady status is occupied at the maximum heat transfer load. The system has an approximately linear tendency to increase the operating temperature, i.e., the saturation temperature, under the effect of the maximum heat transfer capacity. The liquid percentage in the reservoir also shows a tendency to increase when the heat transfer limit is reached, with a liquid content between 0.4 and 0.7. The main reason for the variation in α_{cc} is the variation in the density of the working fluid at different operating temperatures.

Theoretical Comparison Between Ground and Flight Systems

Assuming the vapor–liquid percentage of the components is determined under steady operation, the liquid mass within the CC can be calculated from the mass conservation equation. At each operating temperature, it is assumed that the flat-plate evaporators are completely filled with saturated liquid, and that the VL and LL are filled with vapor and liquid, respectively. The void fraction in the condenser is set at different values at each operating temperature. Therefore, the liquid percentage of the CC can be obtained and the driving force can be calculated in terms of the height difference. Figure 8 shows the theoretical comparison of the driving force of the flight product with the ground equivalent prototype at different void fractions of the working fluid in the condenser. It can be seen from the figure that in the temperature range of -50 °C ~ 50 °C, the driving force of the flight product is always greater than that of the equivalent test prototype. Thus, the heat transfer capacity of the equivalent test prototype under 1 *g* on the earth is smaller than that of the flight product on the moon, thereby making the test result more conservative.

Experimental Setup and Results

Experimental Setup for Ground System

The thermal performance of the equivalent ground prototype is tested in a test chamber, which can provide different temperatures of test environment, from -80℃ to 150℃. A simulated heat source with the same shape as RTG is heated by a DC power supply. The condenser line is coupled with a radiator which can dissipate the heat load into space. During the test, the system is settled on a horizontal trestle. The flat-plate evaporator, RTG simulated heat source, vapor line, liquid line, compensation chamber and control valves are covered with thermal insulation materials to reduce heat leakage. A total of 34 type-T thermal couples are arranged, of which 32 temperature sensors are arranged on the CTPTL system, while two temperature sensors are arranged on the RTG simulated heat source. The locations of the thermal couples are shown in Fig. 9. The temperature measurement range is -196 °C ~ 200 °C with an accuracy of ± 0.1 °C. The temperature data are collected using Agilent 34970A.

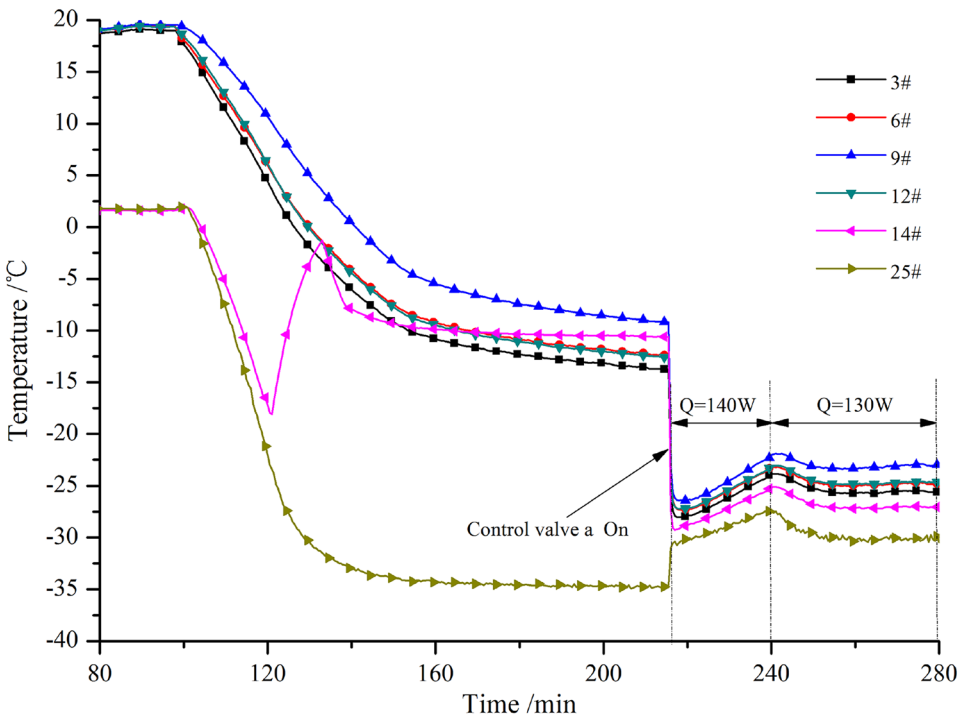

Fig. 10 Temperature variations of thermosyphon loop with time at -30℃

Ground Equivalent Validation

Figures 10, 12 show the test curves of the heat transfer capacity and the temperature variations along the loop system when the two-phase fluid loop works at -30 °C, -20 °C, and -10 °C, respectively. As can be seen from Fig. 14, the initial temperature of Eva and CC is about 18 ℃ and 4 ℃, respectively. As the ambient temperature decreases, the temperature of Eva and CC decreases to -5 ℃ and -33 ℃ slowly. The reason for such a large temperature difference is that both control valves are closed so that the system cannot complete a heat transfer cycle. During the cooling process, it is found that the TC 14 # on VL increases suddenly. The reason is that the liquid in the condenser flows back to the evaporator through the vapor line and that the gravity heat pipe effect appears locally.

At the 215th min, the control valve #1 has been turned on and the two-phase fluid loop has begun operating. The temperature of the flat-plate evaporator drops rapidly, meanwhile the power of 140 W is applied to the RTG simulated heat source. At the 240th min, the temperature of the compensation chamber has increased in excess of -30 °C along with other components. Therefore, the heat source power is turned down to 130 W, and the temperature of the flat-plate Eva and CC decreases to the equilibrium temperature of -31 °C gradually. The average temperature difference of the flat-plate evaporator module and the compensation chamber is about 5.6 °C. It can be concluded that the heat transfer capacity of the thermosyphon loop is above 130 W at the saturation temperature of -30° C.

Proper increasement of the ambient temperature can weaken the radiation ability of the system. So, the thermosyphon loop can be maintained in relatively steady operation under the heat load of 110 W at constant working temperature of -30 ℃. In order to widen the working temperature range, the RTG simulated heat load is increased from 110 to 130 W at the 440th min, as shown in Fig. 11. The temperature of the Eva and CC is increased and stabilized at about -20 °C gradually. The temperature difference between the flat-plate Eva and the CC is 5.4 °C. The heat transfer capacity is no less than 130 W at -20 °C.

In addition, Fig. 12 shows the temperature curve of the system at the operating temperature of about -10 °C. The RTG simulated heat source is adjusted to 130 W at the 196th min and the temperature is gradually leveled off. The temperature difference between the flat-plate evaporator and the compensation chamber is about 5.0 °C, and the heat transfer capacity is no less than 130 W at -10 °C.

The thermal switch characteristics of the thermosyphon loop is another significant feature for the two-phase fluid system. The purpose of setting the control valve is to enable the system to operate or close effectively. At the 500th min in Fig. 11, the CV #1 is shut down so that the temperature of the flat-plate evaporator increases rapidly, indicating that the two-phase fluid loop successfully blocks heat transfer. At the 505th min, the CV #2 is opened so that the temperature of the flat-plate evaporator decreases rapidly, indicating that the two-phase fluid loop restarts successfully. Soon afterwards, shutting down the CV #2 raises the temperature of the Eva again quickly, indicating that the two-phase fluid loop is blocked

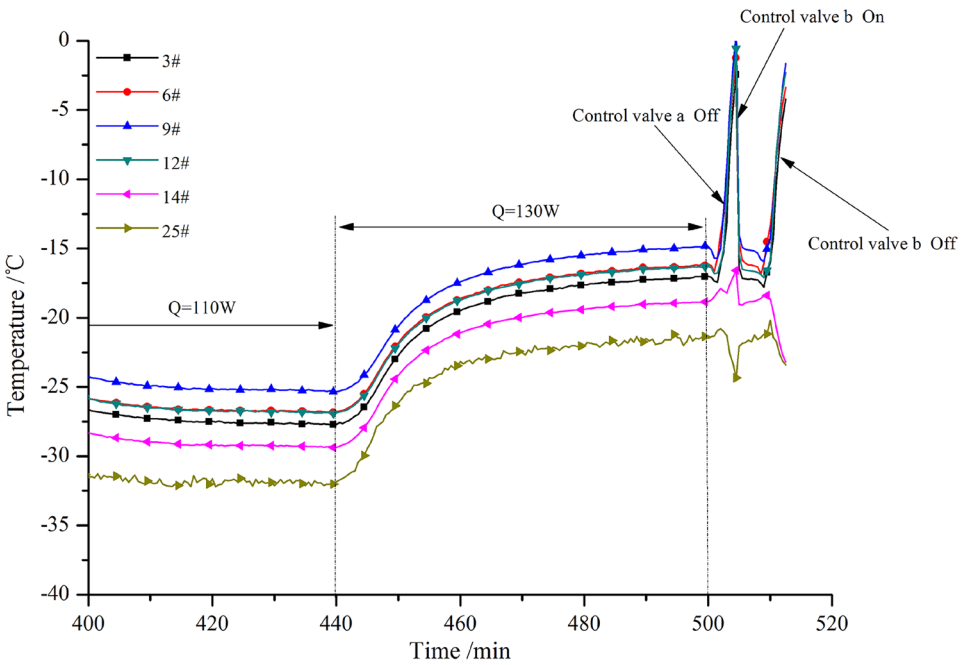

Fig. 11 Temperature variation of two-phase fluid loop with time at the -20℃

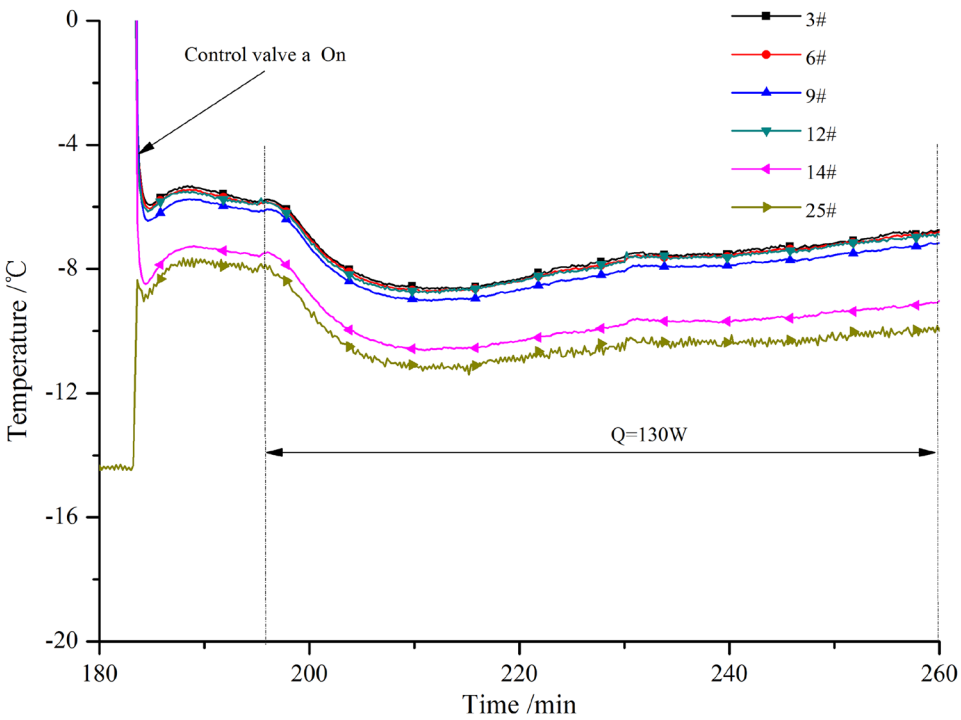

Fig. 12 Temperature variation of two-phase fluid loop with time at the -10℃

again successfully. This awesome function can guarantee the thermosyphon loop for the application on lunar surface.

Figure 13 shows the temperature curve during the high temperature startup of the thermosyphon loop. At the 28th min, the CV #1 is closed to block the system, so that the temperature of the flat-plate evaporator increases sharply. Meanwhile, the heat load remains applied, leading the temperature of TC3, TC6, and TC12 to a high state above 140 °C. Because of the mesh in the evaporator where TC9 is settled and connected into the vapor line, the gravity heat pipe effect is formed between this evaporator and the vapor line. The gas condenses in the VL and flows into the wire

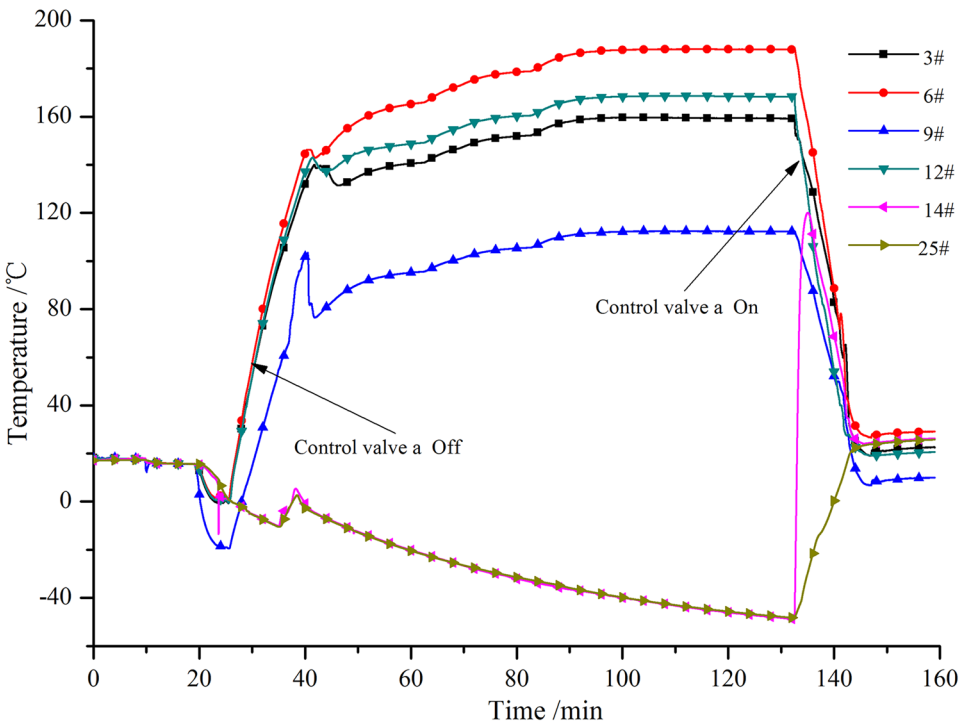

Fig. 13 Temperature curve of two-phase fluid loop during high temperature startup

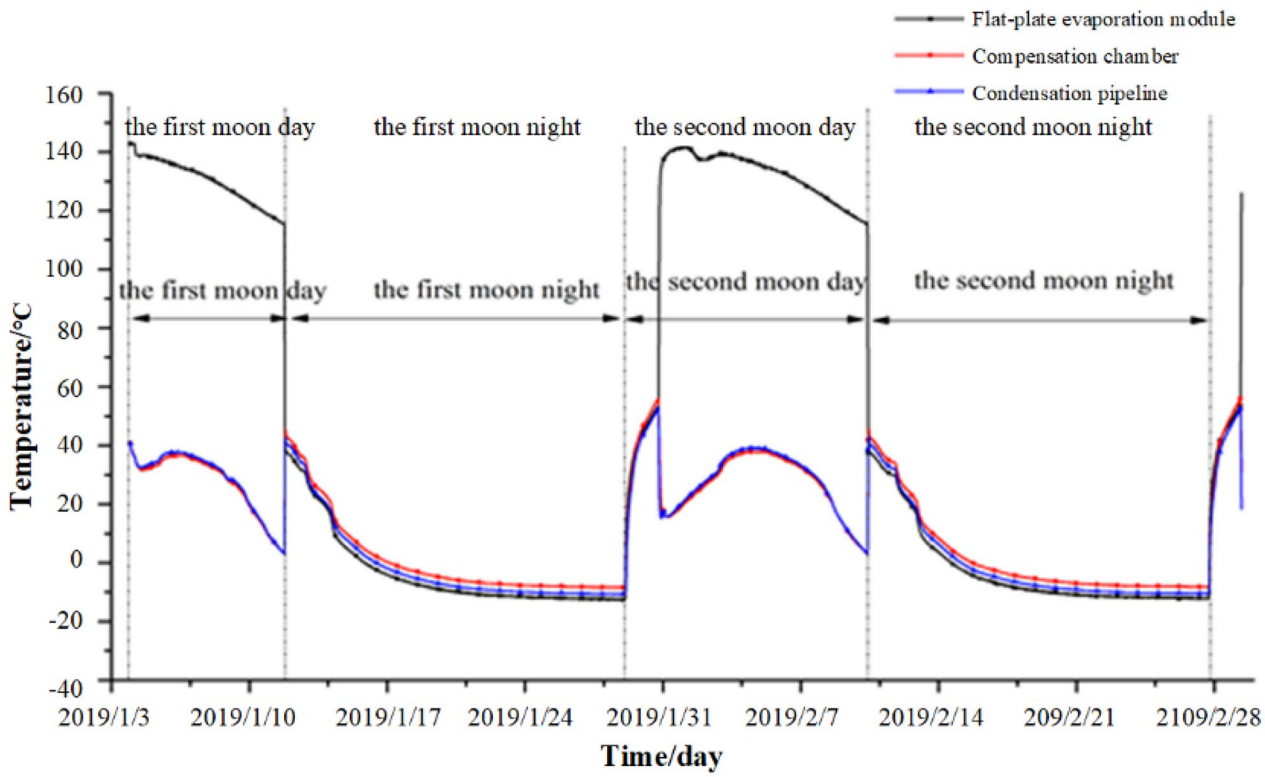

Fig. 14 Temperature variation of CTPTL system with time after landing the moon

mesh evaporator under gravity, so that the temperature of this evaporation channel falls lower than that of the other three channels. When the control valve is opened at the 132th min, the temperature of Eva decreases rapidly, and the temperature of CC increases, indicating a successful high-temperature startup process.

Table 4 shows the test results of the heat transfer capacity and temperature difference of the thermosyphon loop at different operating temperatures. Compared with Table 1, the heat transfer performance of the two-phase fluid loop meets the thermal control requirements of CE-4. The heat transfer capacity in operating temperature -10 ℃ is about 1.5 times of the requirement of 90 W, which meets the criterion of 120% of the requirements. From Fig. 6 it could be known that the heat transfer capacity increases with operating temperature rising, and the temperature difference will be theoretically smaller under the same heat load and higher operating temperature.

Table 4 Heat transfer performance of the equivalent test prototype of the two-phase fluid loop

Temperature /℃	Heat transfer capacity /W	Temperature difference /℃
-30	≥ 130	5.6
-20	≥ 130	5.4
-10	≥ 130	5.0

Performance Validation on Lunar Surface

On December 8, 2018, the two-phase fluid loop was launched with the CE-4 detector, and it landed on the back of the moon on January 3, 2019 successfully. The probe experienced several moon-night cycles and the CTPTL system carried out intermittent work smoothly to meet the thermal control requirements of the lunar probe. Figure 14 shows the time-varying curves of the temperature of the flat-plate evaporator, compensation chamber, and condenser, corresponding to the period from landing on the moon to the second moon night wakeup. As can be seen, the control valves are closed during the moon day, when the temperature of the flat-plate evaporator is as high as 140 °C. When it is the moon night, the control valve is opened to start the CTPTL system quickly, with the temperature of Eva reducing and that of CC increasing rapidly. Therefore, the heat load of RTG can be transferred into the CE-4 detector. During the fourteen-day moon night, the temperature of the CTPTL system gradually decreases and stabilizes at -10 °C. During the wakeup process of the detector, the control valves are closed, and the temperature of the evaporator module rises rapidly, indicating the function of blocking heat transfer is normal.

Conclusion

Specific to the requirements of the moon night preservation and power generation of the CE-4 detector, a technical route of lunar gravity driven thermosyphon loop has been proposed based on flat-plate evaporation module. The structure design, heat transfer capability analysis, ground equivalent verification, and on-orbit validation of the system have been introduced. The main conclusions can be drawn as follows:

1. The function and heat transfer capacity of the gravity-driven thermosyphon loop based on the flat-plate evaporator module have met the thermal control requirements of CE-4 detector;
2. Under different working conditions, the driving force of the ground equivalent test prototype is less than that of the flight product, so that the tested heat transfer capacity tends to be conservative;
3. The heat transfer capacity limit of the ground validation prototype is higher than the required 130 W and increases as the operating temperature rises, but it has not been reached due to the experimental conditions;
4. It can be known from the orbit telemetry temperature data that the two-phase fluid loop operates stably during the moon-night cycle. The switch function of the system is normal, which has guaranteed stable operation of the CTPTL system in each cycle.

Acknowledgements This work is supported by the Chinese lunar exploration program.

Declarations

Competing Interest The authors declare that they have no known competing financial interests.

References

Benaroya, H.: Lunar habitats: A brief overview of issues and concepts. Reach. **7**, 14–33 (2017)

Dittus, F.W., Boelter, L.M.K.: Heat transfer in automobile radiators of the tubular type. Int. Commun. Heat Mass Transfer **12**, 3–22 (1985)

Fateri, M., Pitikaris, S., Sperl, M.: Investigation on wetting and melting behavior of lunar regolith simulant for additive manufacturing application. Microgravity Sci. Technol. **31**, 161–167 (2019)

Fraser, S.D.: Theory and applications of cooling systems in lunar surface exploration. In: Moon. pp. 405–437. Springer (2012)

He, J., Lin, G., Bai, L., Miao, J., Zhang, H., Wang, L.: Effect of non-condensable gas on startup of a loop thermosyphon. Int. J. Therm. Sci. **72**, 184–194 (2013). https://doi.org/10.1016/j.ijthermalsci.2013.05.009

He, J., Lin, G., Bai, L., Miao, J., Zhang, H., Wang, L.: Effect of non-condensable gas on steady-state operation of a loop thermosyphon. Int. J. Therm. Sci. **81**, 59–67 (2014). https://doi.org/10.1016/j.ijthermalsci.2014.03.001

Hu, W., Long, M., Kang, Q., Xie, J., Hou, M., Zhao, J., Duan, L., Wang, S.: Space experimental studies of microgravity fluid science in China. Chin. Sci. Bull. **54**, 4035–4048 (2009)

Jaworske, D.A., McCollum, T.A., Gibson, M.A., Sanzi, J.L., Sechkar, E.A.: Evaluating Heat Pipe Performance in 1/6 g Acceleration: Problems and Prospects. (2011)

Khodabandeh, R., Furberg, R.: Heat transfer, flow regime and instability of a nano- and micro-porous structure evaporator in a two-phase thermosyphon loop. International J. Thermal Sci. **49**, 1183–1192 (2010a)

Khodabandeh, R., Furberg, R.: Instability, heat transfer and flow regime in a two-phase flow thermosyphon loop at different diameter evaporator channel. Appl. Thermal Eng. **30**, 1107–1114 (2010b)

Kim, T.Y.: Thermal shelter for survival of rover during cryogenic lunar night. Acta Astronaut. **171**, 151–155 (2020)

Lemmon, E.W., Bell, I.H., Huber, M.L., McLinden, M.O.: NIST Standard Reference Database 23: Reference Fluid Thermodynamic and Transport Properties-REFPROP, Version 10.0, National Institute of Standards and Technology. Standard Reference Data Program, Gaithersburg. (2018)

Li, J., Lin, F., Niu, G.: An insert-type two-phase closed loop thermosyphon for split-type solar water heaters. Appl. Therm. Eng. **70**, 441–450 (2014)

Lockhart, R.W.: Proposed correlation of data for isothermal two-phase, two-component flow in pipes. Chem. Eng. Prog. **45**, 39–48 (1949)

Palos, M.F., Serra, P., Fereres, S., Stephenson, K., González-Cinca, R.: Lunar ISRU energy storage and electricity generation. Acta Astronaut. **170**, 412–420 (2020)

Plachta, D.W., Sutherlin, S.G., Johnson, W.L., Feller, J.R., Jurns, J.M.: Methane lunar surface thermal control test. (2012)

Pletser, V.: Microgravity research conducted by Prof. JC Legros during parabolic flights: notes on a historical perspective. Microgravity Sci. Technol. **31**, 445–463 (2019)

Reitz, B., Lotz, C., Gerdes, N., Linke, S., Olsen, E., Pflieger, K., Sohrt, S., Ernst, M., Taschner, P., Neumann, J.: Additive manufacturing under lunar gravity and microgravity. Microgravity Sci. Technol. **33**, 1–12 (2021)

Samba, A., Louahlia-Gualous, H., Le Masson, S., Nörterhäuser, D.: Two-phase thermosyphon loop for cooling outdoor telecommunication equipments. Appl. Therm. Eng. **50**, 1351–1360 (2013)

Sarno, C., Tantolin, C., Hodot, R., Maydanik, Y., Vershinin, S.: Loop thermosyphon thermal management of the avionics of an in-flight entertainment system. Appl. Therm. Eng. **51**, 764–769 (2013)

Shah, M.M.: A correlation for heat transfer during condensation in horizontal mini/micro channels. Int. J. Refrig **64**, 187–202 (2016)

Simonsen, L.C., DeBarro, M.J., Farmer, J.T.: Conceptual design of a lunar base thermal control system. In: NASA. Johnson Space Center, The Second Conference on Lunar Bases and Space Activities of the 21st Century, Volume 2 (1992)

Sridhar, K.R., Gottmann, M.: Lunar base thermal control systems using heat pumps. Acta Astronaut. **39**, 381–394 (1996)

Stephan, R.: Overview of the Altair lunar lander thermal control system design. In: 40th International Conference on Environmental Systems. p. 6080 (2009)

Sukchana, T., Pratinthong, N.: Effect of bending position on heat transfer performance of R-134a two-phase close loop thermosyphon with an adiabatic section using flexible hoses. Int. J. Heat Mass Transf. **114**, 527–535 (2017)

Tong, Z., Liu, X.-H., Jiang, Y.: Experimental study of the self-regulating performance of an R744 two-phase thermosyphon loop. Appl. Energy **186**, 1–12 (2017)

Zhang, H., Miao, J., Wang, L., Mo, Q., Liu, Z., Xiang, Y.: Ground test method and results of closed two-phase thermosyphons for the moon

exploration spacecraft Chang'E-3 (in Chinese). Science China Technology. **44**, 589–596 (2014)

Zhang, P., Shi, W., Li, X., Wang, B., Zhang, G.: A performance evaluation index for two-phase thermosyphon loop used in HVAC systems. Appl. Therm. Eng. **131**, 825–836 (2018)

Zhang, S., Wang, L., Bai, Y., Lin, X., Peng, L., Chen, H.: Experimental and theoretical analysis of a closed loop two-phase thermosiphon under various states for latent heat storage. Energy Rep. **6**, 1–7 (2020)

Zhao, J.: Two-phase flow and pool boiling heat transfer in microgravity. Int. J. Multiph. Flow **36**, 135–143 (2010)

Zhao, J., Li, Z., Miao, J., Zhang, H., Xiang, Y., Zhang, L., Du, W.: Numerical simulation of heat transfer in closed two-phase natural circulation system driven by partial gravity (in Chinese). Manned Spaceflight. **21**, 64–68 (2015)

Zhao, J., Xie, J., Lin, H., Hu, W., Ivanov, A.V., Belyaev, A.Y.: Microgravity experiments of two-phase flow patterns aboard MIR space station. Acta. Mech. Sin. **17**, 151–159 (2001)